Ralph J. Roberts
CENTER FOR RESEARCH
IN
ECONOMIC GEOLOGY

ANNUAL RESEARCH MEETING-1998

Program and Reports

7-8 January 1999
Midby-Byron Building
Room 107-109
University of Nevada, Reno
Reno, NV 89557

Ralph J. Roberts
Center for Research in Economic Geology

1998 Annual Report

Ore Mineralogy, Alteration, and Fluid Inclusion Studies at the Getchell and Turquoise Ridge Deposits, Northern Nevada

Jean S. Cline, Associate Professor,
Tracy Cail, Michiko Shigehiro, and Kelli Weaver, Graduate Students
University of Nevada, Las Vegas

INTRODUCTION

This project consists of three separate studies which are being conducted by Tracy Cail, Michiko Shigehiro, and Kelli Weaver, graduate students, under the direction of Jean S. Cline, at the University of Nevada, Las Vegas. All three students are enrolled in the M.S. program and are supported by research or teaching assistantships at UNLV. Cail's project involves examining the trace, minor, and major element geochemistry and alteration mineralogy associated with gold mineralization at the Getchell underground deposit. Shigehiro's study will provide paragenetic, fluid inclusion microthermometric, and fluid inclusion oxygen and hydrogen isotope data for the Turquoise Ridge deposit. Weaver is conducting a detailed trace element and sulfur isotope study of ore and non-ore pyrite in the Getchell underground deposit. The alteration study began last spring; the fluid inclusion and pyrite geochemistry studies are nearing completion.

The Getchell district is located 72 km northeast of Winnemucca, Nevada, on the east flank of the Osgood Mountains. Mining of three open pits terminated in 1995 following production of 1.2 million ounces gold averaging 0.181 ounces/ton (DeLong, 1996). Gold is currently produced by underground mining of deep ore located beneath the old pits in the footwall of the Getchell fault. The Turquoise Ridge deposit, located northeast of the Getchell deposit, is under development with production anticipated early in 1999. Proven and probable reserves at the Getchell Underground and Turquoise Ridge deposits, at the end of 1997, totaled 6.1 million contained ounces with an average grade of 0.379 ounces/ton (Tingley and LaPointe, 1998).

The Getchell district provides an excellent opportunity for the current studies owing to the presence of fine to moderately coarse-grained and unoxidized, replacement and open-space-filling ore assemblages, that precipitated along major fault zones. A well-constrained mineral paragenesis has been defined for the Getchell deposit (Cline et al., 1997; Cline, in review); preliminary work at Turquoise Ridge (Groff, 1996) indicates that similar textural features are present in this system.

TURQUOISE RIDGE FLUID INCLUSION STUDY

Project Goals

The primary objectives of this study are to examine ore-stage minerals and related fluid inclusion assemblages at the Turquoise Ridge gold deposit, to improve our understanding of the gold depositional system. This study will provide detailed studies of the mineral paragenesis, fluid inclusion microthermometry, and oxygen and hydrogen

isotopic ratios of fluid inclusions. Three questions are addressed: (1) At what pressures and temperatures did the deposit form? (2) What is the ore mineral paragenesis? (3) What are the sources of ore fluids?

Introduction

The Turquoise Ridge gold deposit is a recently discovered, deep, high-grade system located 600 m northeast of the shallower, lower grade Getchell deposit. Gold mineralization was discovered at Turquoise Ridge in 1994 as a part of an extensive mapping program at the Getchell deposit. Ore bodies are developed in Paleozoic silt- or clay-rich calcareous dolomite and limestone units dissected by the high-angle faults (Berentsen et al., 1996). This deposit provides an excellent opportunity to investigate a Carlin-type gold deposit because of the presence of fine- to moderately coarse-grained mineralization containing fluid inclusions and exhibiting textural relationships that provide paragenetic information (Groff, 1996).

Sampling

Approximately six hundred samples from seventeen drill holes along section 300 of the Turquoise Ridge deposit (Fig. 1) were collected during June, 1997. This section cuts through a central zone of high grade mineralization representative of the Turquoise Ridge deposit. Minerals and textural relationships in assayed core samples were examined to determine the mineral paragenesis and to identify assemblages of non-ore and ore-stage minerals. These studies indicated that iron-sulfide minerals associated with gold are arsenic-rich and fine-grained, while subhedral to euhedral pyrite grains are present in non-ore samples. These and other textures and assays were used to identify ore-stage minerals and assemblages, and to select samples for polished thin section and doubly polished section preparation for petrographic and fluid inclusion studies.

Polished thin sections, doubly polished thick sections, and quick plates were prepared from samples from 16 drill holes along section 300. Sections were prepared from twenty-two samples from drill hole 94-172, collected along transects from non-ore through ore grade material. This core was relatively intact and sampling covered an interval of approximately four hundred feet. Examination of these transects permits variations in the mineral assemblages, which reflect increasing ore grade rather than lithological changes, to be identified. Polished thin sections were prepared from seven samples of low-grade material and non-ore iron-sulfide minerals. Fifteen doubly polished thick sections were prepared for petrography and fluid inclusion studies of non-ore and ore stage specimens.

Doubly polished sections for petrography and fluid inclusion analyses were prepared from high-grade samples from seven additional drill holes along section 300, including a remarkably high-grade interval from drill hole 95-122, that assayed 4.71 ounces/ton gold. An additional forty-three quick plates were prepared from fifteen different drill holes along the section 300 fence. These quick plates were used to identify the location and distribution of ore-stage jasperoid quartz, the presence of fluid inclusions, and details in petrography. The quick plates have not been used for microthermometric studies owing to insufficient optical clarity.

Petrographic and Paragenetic Studies

Ore is hosted by two types of variably metamorphosed sedimentary rocks at the Turquoise Ridge deposit; brown hornfels hosts ore at shallow levels, and black hornfels hosts ore at deeper levels. Ore-bearing brown hornfels is clay-rich and exhibits alternating bands of clay minerals and protolith. Black hornfels is relatively competent and contains graphite; clay bands are absent in black hornfels.

Preliminary electron microprobe studies confirmed the presence of gold in fine-grained pyrite that forms porous rims on earlier formed pyrite; gold is not present in coarser, euhedral to subhedral pyrite grains. Pyrite in high-grade samples is rich in trace metals, particularly arsenic. Iron sulfides in non-ore brown and black hornfels vary;

brown hornfels contains pyrite and pyrrhotite, while marcasite is dominantly present in black hornfels. Petrographic studies indicate successive deposition of (1) pyrite with gold, (2) jasperoid quartz, (3) orpiment, (4) realgar, and (5) calcite.

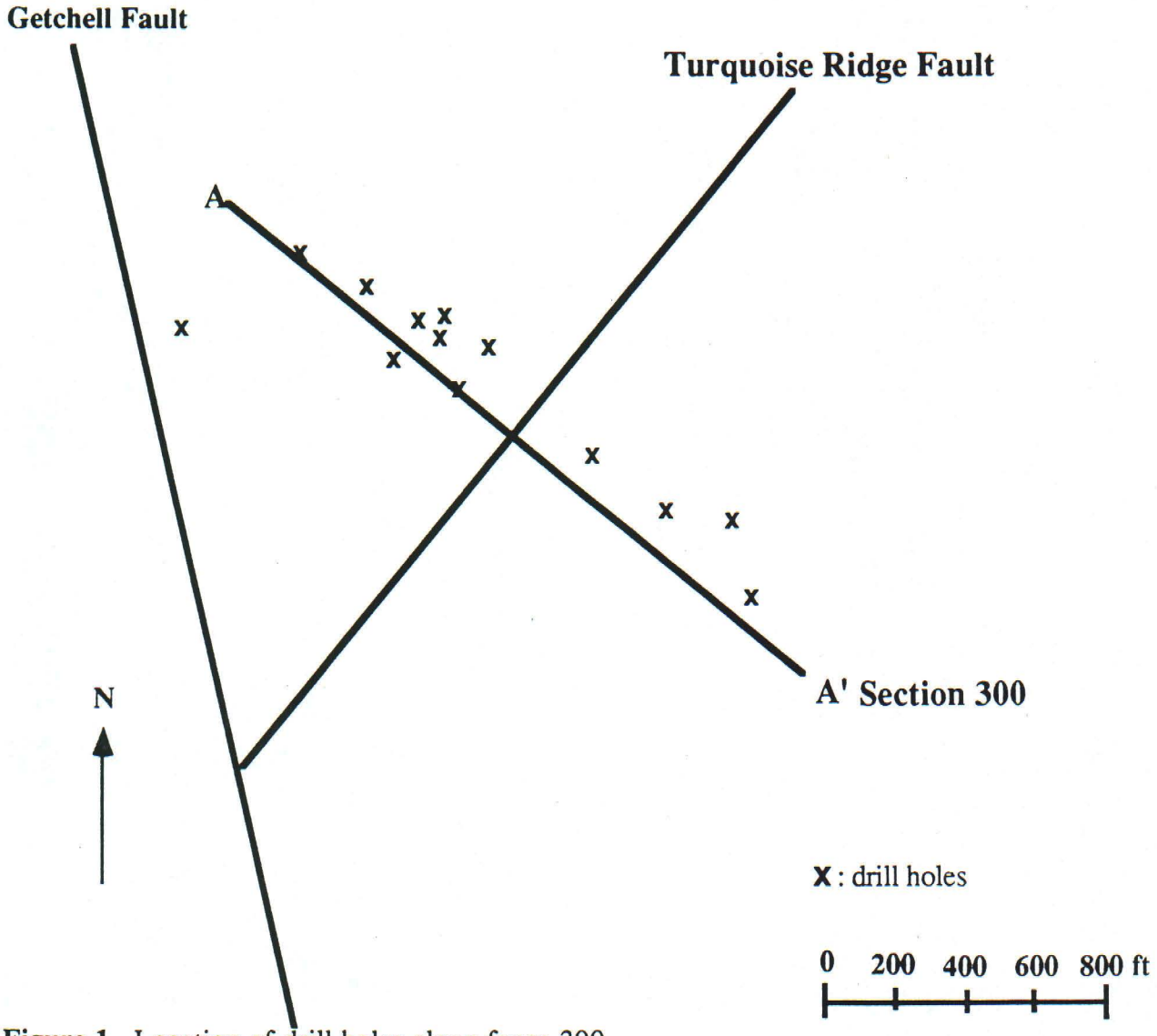

Figure 1. Location of drill holes along fence 300.

At least two distinctively different types of quartz are present in ore-grade and non-ore grade samples. Quartz containing small calcite inclusions generally forms microcrystalline grains and exhibits a typical jasperoid texture. These textures indicate that jasperoid quartz has replaced calcite. A second type of quartz is present as clasts in ore-grade samples and veins in non-ore-grade black hornfels. In veins, this quartz forms coarse euhedral crystals indicating open space quartz precipitation. In clasts in ore-grade samples, this quartz is euhedral, but fractured. Both veins and clasts contain similar fluid inclusion assemblages, which are distinctly different from inclusions trapped in jasperoid. The grain size, crystal shapes, and fluid inclusions suggest that quartz in veins and clasts formed under the same conditions. Paragenetic constraints indicate that this quartz is pre-ore, and spatial and textural relationships suggest that it may be related to intrusion of a 90 Ma granodiorite (Silberman et al., 1974).

Gold-bearing, fine pyrite grains are consistently present both within jasperoid quartz grains, and along pre-ore quartz and jasperoid quartz grain boundaries. These textural relationships suggest that gold mineralization occurred prior to, and is associated with jasperoid quartz precipitation. Preliminary electron microprobe data, ore microscopy, and petrographic studies suggest close timing of gold, pyrite, and jasperoid quartz precipitation. However, jasperoid quartz grains that do not contain pyrite are also present, indicating that jasperoid quartz formed prior to and possibly after gold precipitation.

Orpiment, realgar, and calcite comprise a late ore-stage assemblage. Orpiment contains euhedral jasperoid quartz, and realgar precipitated on orpiment crystal surfaces. Calcite filled open spaces between realgar, orpiment and jasperoid quartz. Intensely altered ore-grade brown hornfels contains abundant realgar. Orpiment has not been identified in ore-grade samples.

A high grade sample from TR 95-122 contains coarse clay grains, which reach 330 micrometers in diameter. Birefringence is low and petrographic features suggest that the clay may be kaolinite. The clay contains euhedral jasperoid quartz and fine ore-stage pyrite grains; outer crystal faces of the clay were subsequently overgrown by realgar. These textural relationships show that the clay formed after pyrite-gold-jasperoid mineralization, but prior to realgar precipitation, indicating that the clay formed as part of the mineralizing hydrothermal event. X-ray analyses are being conducted to identify this mineral.

Microthermometric Studies

Fluid inclusion assemblages (Goldstein and Reynolds, 1994), which contain multiple inclusions with consistent phase ratios, were examined during this study. Inclusions were identified as (1) primary, by presence in a growth zone or attachment to a solid inclusions, (2) secondary, by presence in a healed fracture, (3) pseudosecondary, by presence in a healed fracture within a single grain, or (4) unknown. Pre-ore quartz, gold-bearing jasperoid, non-ore jasperoid, and realgar and calcite were examined for fluid inclusion assemblages.

Fluid Inclusion Microthermometry: A Linkam TH 600 stage and Olympus BX60 microscope were used to collect microthermometric data. With this system, ice melting temperatures of small inclusions can be observed at a magnification of 1280x (80x objective, 1.6x magnifier, 10x oculars). 800x magnification is adequate for measurement of homogenization temperatures.

During freezing studies, the stage was cooled to -196°C. As the sample is heated to within ~10°C of the ice melting temperature, the heating rate is decreased to 5°C/minute. The temperatures is cycled to determine the ice melting temperature to within 0.1°C. Homogenization temperatures were determined for all inclusions in each chip during a single heating run, to prevent inclusion stretching. A heating rate of 5°C/minute was used when the vapor phase became small.

Sections were prepared for microthermometry by cutting into approximately 5 mm x 5 mm chips. Because of the vuggy nature of the samples and fear of losing tiny fragments of chips containing inclusions, many chips were not removed from the glass slides. This led to visibility problems during heating of the chips when the glue started to melt. Because of this problem, some homogenization temperatures could not be obtained.

Fluid inclusions in pre-ore quartz are commonly ~ 5 micrometers in diameter and are suitable for microthermometry. These clear quartz crystals contain abundant primary inclusions in their cores; most inclusions in pre-ore quartz, however, have an unknown origin. Inclusions yield a wide range of salinities (Fig. 2) and homogenization temperatures (Fig. 3). Salinities range from 0 to 24 wt.% NaCl equivalent, with a mode between 6 and 10 wt.%. Homogenization temperatures range from 100° to 300°C, however, most inclusions homogenize between 140° and 220°C. The wide range in salinities and homogenization temperatures likely reflects trapping of a variety of fluids over a potentially lengthy period of time.

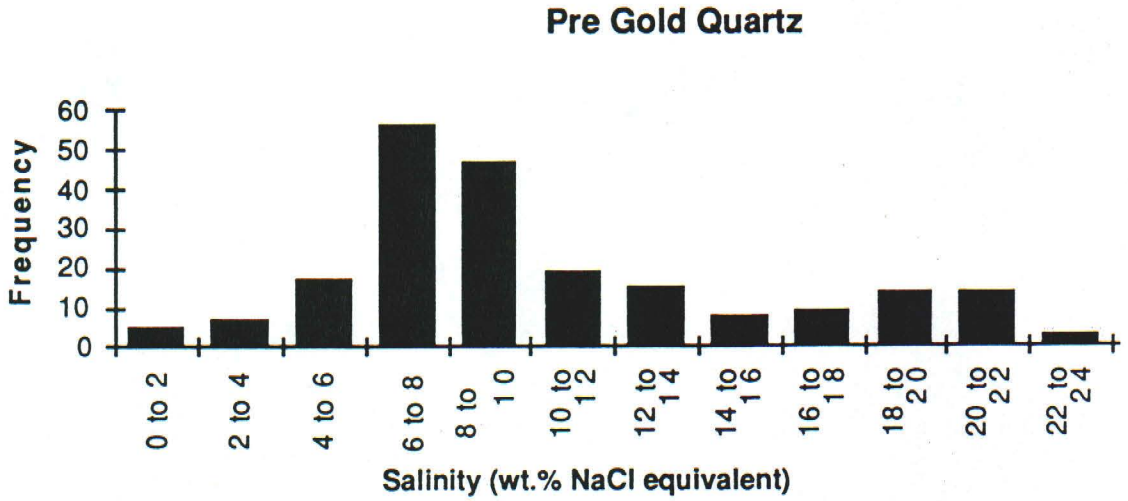

Figure 2. Salinities of fluid inclusions in pre-ore quartz.

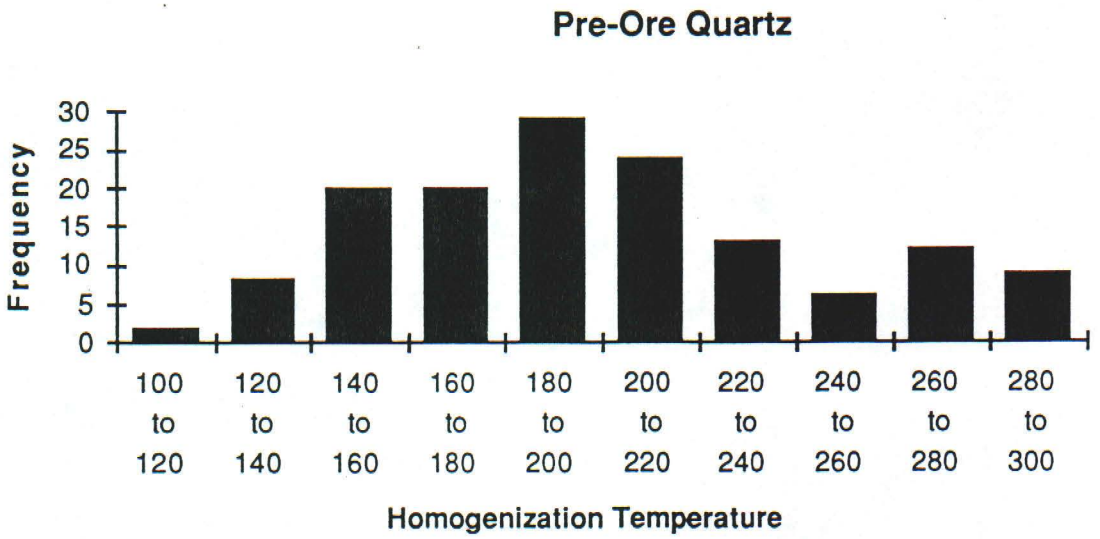

Figure 3. Homogenization temperatures of fluid inclusions in pre-ore quartz.

Fluid inclusions in jasperoid quartz are generally less than 2.5 micrometers in diameter and the majority of these inclusion are too small for microthermometric studies. Most inclusions are two-phase, liquid-dominant, with a vapor bubble occupying 5 to 10 volume percent of the inclusion. Origins of these inclusions are generally unknown or secondary; however, a few inclusions have been identified within growth zones.

Salinities and homogenization temperatures of jasperoid quartz exhibit greater consistency than pre-ore quartz. Salinities in jasperoid quartz range from 2 to 22 wt.% NaCl equivalent (Fig. 4), however, most inclusions have salinities between 6 and 10 wt.%. Homogenization temperatures range from 100° to 240°C (Fig. 5) and most inclusions homogenization between 160° and 220°C. These data suggest that ore-stage fluids had minimum temperatures in the range of 160° to 220°C and salinities between 6 and

10 wt.% NaCl equivalent. Homogenization temperatures are consistent with temperatures determined for the Getchell deposit; however, salinities are somewhat higher than salinities of 4 to 6 wt.% NaCl equivalent determined for the Getchell open pit mine (Cline, in review).

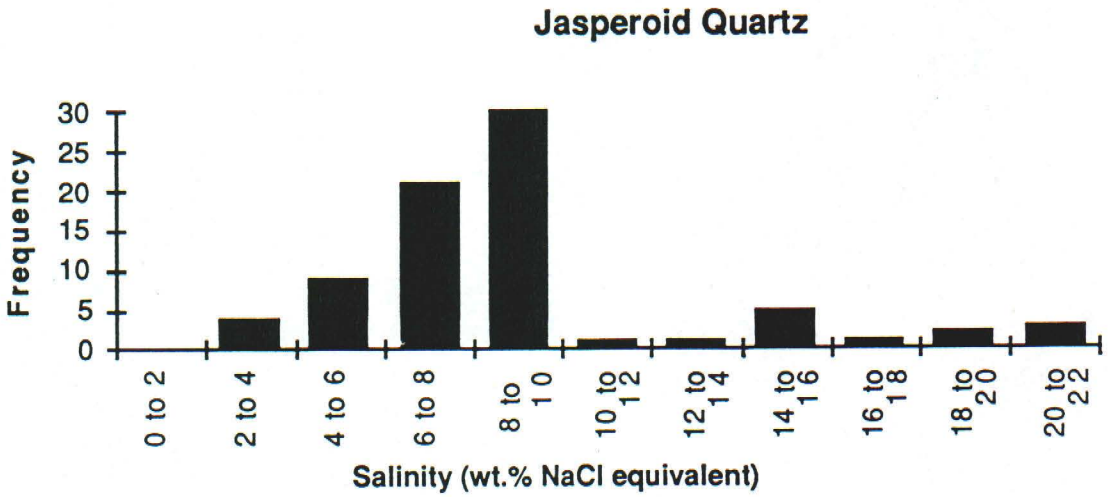

Figure 4. Salinities of fluid inclusions in jasperoid quartz.

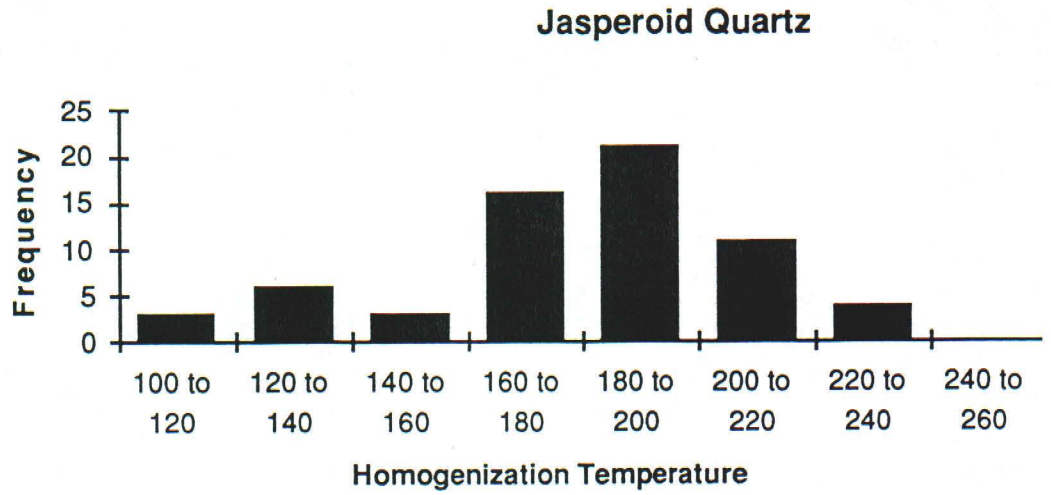

Figure 5. Homogenization temperatures of fluid inclusions in jasperoid quartz.

Microthermometry of primary inclusions in quartz, which trapped ore-stage pyrite as it precipitated, will provide temperature and salinity constraints for fluids that clearly precipitated ore-stage mineralization. Figures 6a and 6b show a cross section of a euhedral quartz crystal, under reflected and transmitted light, respectively, that contains ore-stage pyrite, and primary fluid inclusions in growth zones. The six encapsulated pyrite grains were analyzed by electron microprobe to quantify Au and trace metal concentrations. Figure 6a shows locations of pyrite grains and Au and As

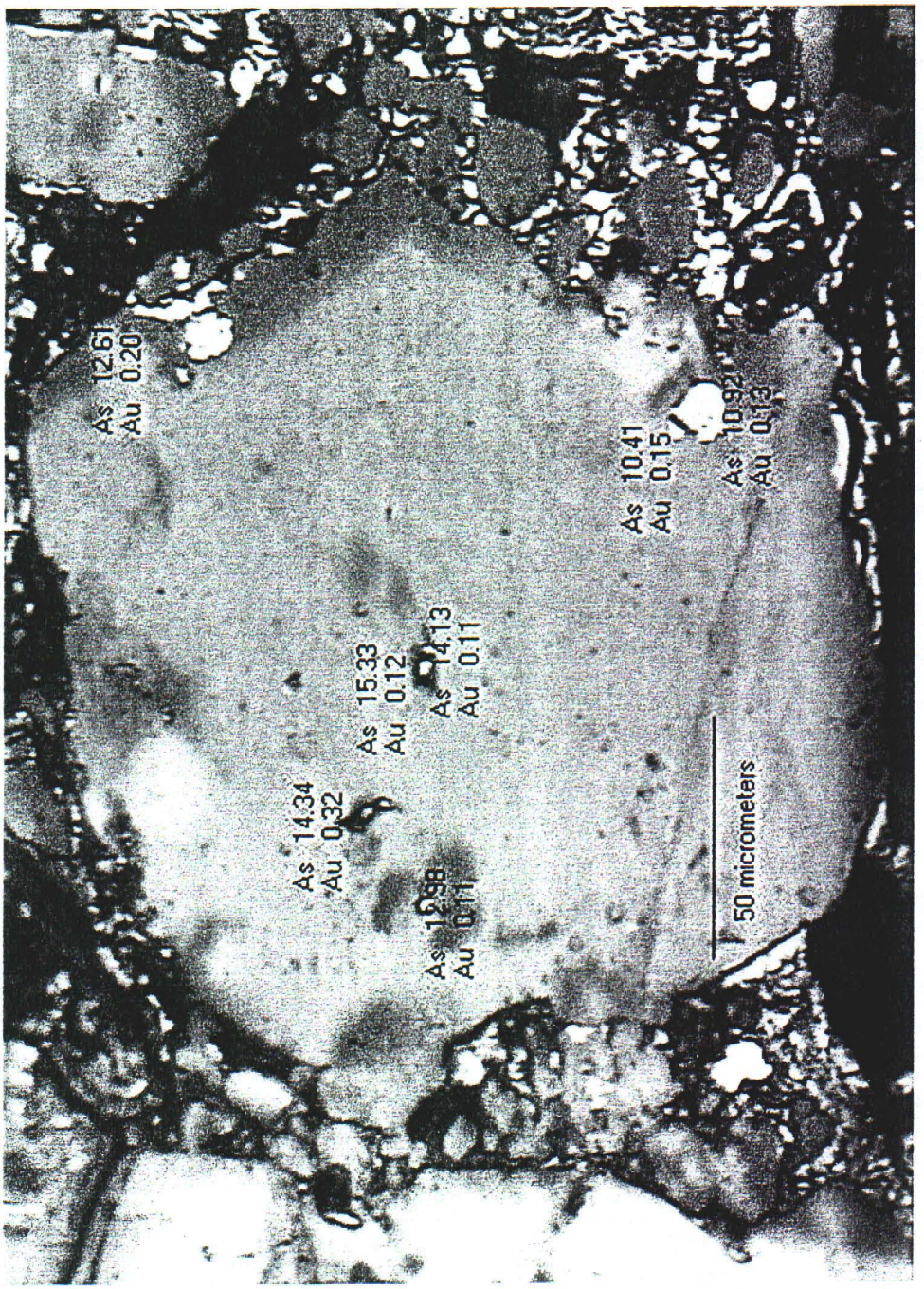
As 12.61
Au 0.20
As 14.34
Au 0.32
As 15.33
Au 0.12
As 14.13
Au 0.11
As 12.98
Au 0.11
As 10.41
Au 0.15
As 10.92
Au 0.13
50 micrometers

Figure 6A

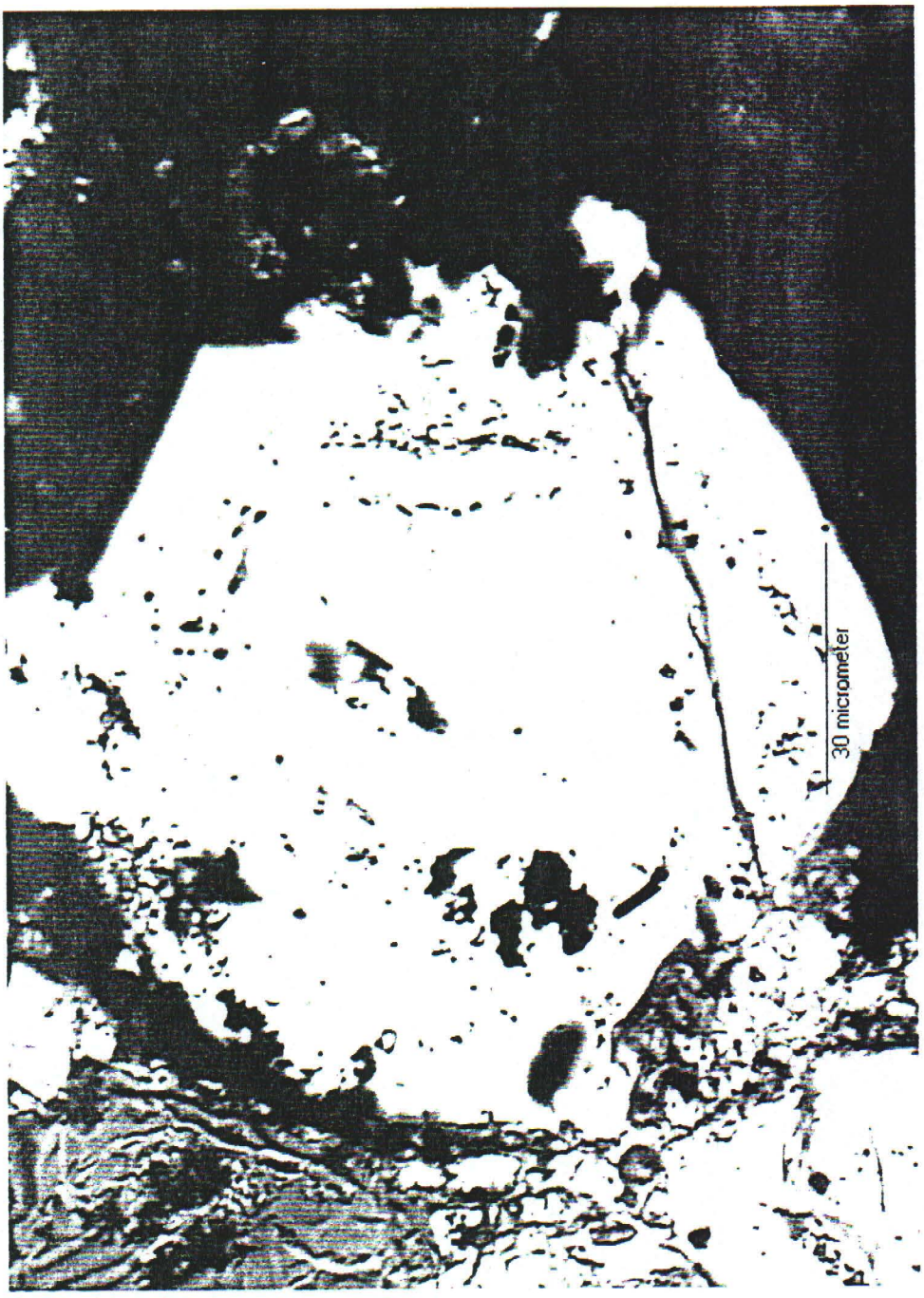

Figure 6B

analyses for each grain in weight percent. The high As and Au values confirm that these are ore-stage pyrite grains. The same crystal at the same orientation is shown in figure 6b. The irregular dark, spotty bands, which parallel the crystal rim, are growth zones containing primary fluid inclusions. Microthermometric studies of these inclusions are now underway.

Future Research

Microthermometric studies will be completed in January of 1999. Quartz separates of both jasperoid and pre-ore quartz, are now being prepared for oxygen and hydrogen isotope analyses of inclusion fluids, to identify fluid sources. Data will be compiled and evaluated and a manuscript describing the paragenetic, fluid inclusion, and stable isotope studies will be prepared for publication.

PYRITE GEOCHEMISTRY STUDY

Project Goals

The goals of this project include: 1) identify the trace metal concentrations in gold-bearing iron sulfide grains, 2) identify the trace metal contents of igneous and diagenetic pyrite grains, 3) identify the location of, and quantify, gold in pyrite and marcasite, and 4) obtain preliminary sulfur isotopic analyses, which will reflect geologic processes responsible for pyrite precipitation.

Sampling Location and Gold Occurrences

Sample locations in the northwest, main, and south ore zones of the Getchell underground mine are illustrated in long section in figure 7. Samples were collected from production drill core and warehoused material. The northwest zone has yielded the highest-grade ore. Abundant silicified and mineralized high-grade drill core samples from this zone had been archived and were available for this study in addition to production core, which provided abundant high grade material. At the time of sample collection, thc main zone was not actively being mined and a limited amount of warehoused samples were available for collection. Exploration of the south zone was just beginning and samples were collected from available production core; no samples had been warehoused. Thus, the number of samples from the main and south zones is limited and 47% of the samples collected containing high grade (>0.1 wt.%) gold are from the northwest zone of the mine. Although ore-stage pyrite was present in samples from throughout the mine, the pyrite samples yielding the largest, and most trace-element enriched pyrite rims originated from the northwest region.

Analytical Procedures

Analyzed samples include mineralized and unmineralized sedimentary and igneous rocks, and were collected from transects through low-grade to high-grade ore zones. Thirty-two thin sections were evaluated petrographically and twenty-two were analyzed using an electron microprobe. Electron microprobe analyses (EMPA) determined concentrations of Fe, S, Pb, Co, Hg, Ag, Tl, Ni, As, Au, Cu, Sb, Zn, and Mo in gold-bearing and barren pyrites.

Trace-Element Studies

Several types of pyrite have been distinguished through differences in morphology, chemistry, and trace-element compositions. EMPA indicate that major element Fe and S, and trace element Tl, Sb, Cu, As, and Hg concentrations correlate with pyrite morphology and gold concentration. Three types of high-grade, gold-bearing pyrite are present and occur as 1) framboids in jasperoid quartz groundmass, 2) sharp rims and 3) faintly discernible "gradual" rims. Both types of rims envelop low-grade, pre-ore pyrite. These

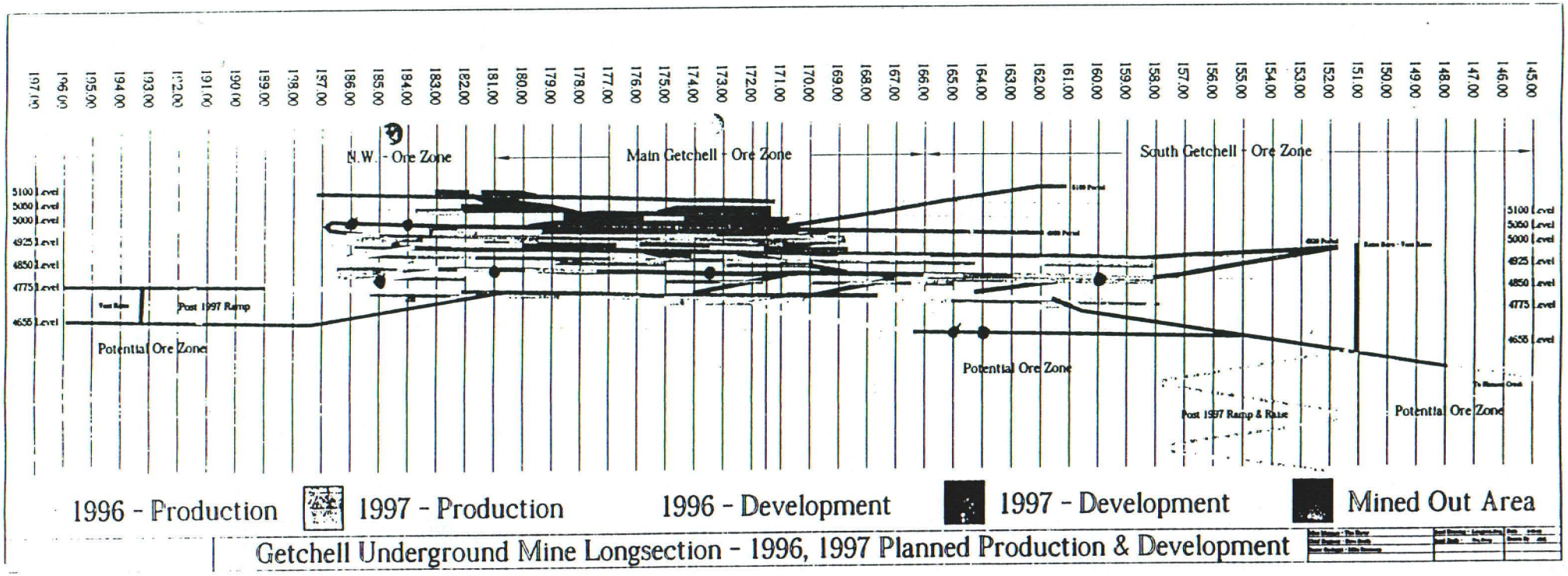

Figure 7. Sample locations (●) in the northwest, main, and south ore zones of the Getchell underground mine.

high-grade, ore-stage pyrites contain elevated Hg, Tl, As, Sb, Cu, and Au and trace to nil Pb, Co, and Ni. Low-grade, pre-ore and post-ore pyrite contains nil to minor Hg, Tl, As, Sb, Cu, and Au, nil to trace Pb, Co, and Ni, and near stoichiometric Fe and S. We presently identify seven populations of pyrite that formed during at least three different stages.

Stage 1: pre gold ore stage: (0.0 ounces/ton Au)

Pyrite morphologies: Stage 1 mineralization contains two morphologies of pyrite. Type 1 is associated with intrusions and dikes (Fig. 8A). The second type of pyrite, Type 2, is associated with metasedimentary rocks and may be diagenetic (Fig. 8B). Both of these pre-gold ore, low-grade, pyrites exhibit typical cubic forms; they are generally subhedral in shape, take a high polish, exhibit high relief, and are bright yellowish-white in color.

Pyrite Geochemistry: Stoichiometric Fe and S, low to nil Tl, Au, Sb, Cu, As, and Hg, low, nil or trace Co, Pb and Ni (Table 1).

Stage 2: gold ore stage: (>0.1 ounces/ton Au)

Pyrite morphologies: Stage 2 mineralization commonly consists of three morphologically and chemically distinct populations of sulfides.

Type 3: High-grade pyrite/marcasite rims with low relief, poor polish, slightly brownish yellow, anhedral "fuzzy" appearance; often surrounds euhedral to subhedral Type 2 core sulfides (Table 1), forms a sharp distinguishable contract with cores (Fig. 8C).

Type 3 Geochemistry: Less than stoichiometric Fe and S, high Tl, Au, Sb, Cu, As, Hg, and trace to nil Co, Pb, and Ni (Table 1).

Type 4: High-grade pyrite/marcasite framboid-like grains. Low relief, slightly brownish yellow, spherical "fuzzy puff-ball" appearance. Type 4 sulfides typically occur as very small (5 micrometer) fuzzy sulfide grains trapped between jasperoid crystal faces (Fig. 8D), and are often aggregated into rims surrounding Type 2 sulfide cores.

Type 4 Geochemistry: Less than stoichiometric Fe and S, high Tl, Au, Sb, Cu, As, Hg and trace to nil Co, Pb, and Ni (Table 1).

Figure 9 illustrates a back scattered electron image and elemental maps of Fe, S, Ni, Hg, Sb, Tl, and As, for Type 2 pyrite rimmed by Type 3 overgrowths, and disseminated high-grade Type 4 pyrite. Note the inverse correlation between Fe and S, and Hg, Sb, Tl, and As, and the lack of correlation of other elements with Ni.

Type 5: Very high-grade pyrite/marcasite rims. High relief, anhedral, very slightly yellowish to brownish yellow in color, faint, almost indistinguishable from the Type 2 cores under reflected light, but very visible under backscatterd electron imaging. Core edges appear rounded (Fig. 8E).

Type 5 Geochemistry: Significantly less than stoichiometric Fe and S, highest Au, Cu and As, high Tl, Sb, and Hg, and trace to nil Co, Pb, and Ni (Table 1). Additionally, the cores contain elevated As (Table 1).

Figure 10 illustrates a back scattered electron image and trace element maps of S, Fe, As, Hg, Sb, Tl, and Au, for Type 5 high-grade rims on Type 2 non-ore pyrite cores. Note the rounded form of the pyrite cores, the strong correlation between As, Hg, Sb, Tl, and Au, and the inverse correlation between these ore-stage elements and S and Fe.

Type 6: Low to medium grade pyrite/marcasite, subhedral to anhedral masses, often fractured, and range from whitish yellow to yellowish brown in color, irregular edges (Fig. 8F).

Figure 8. *Pyrite Morphologies*

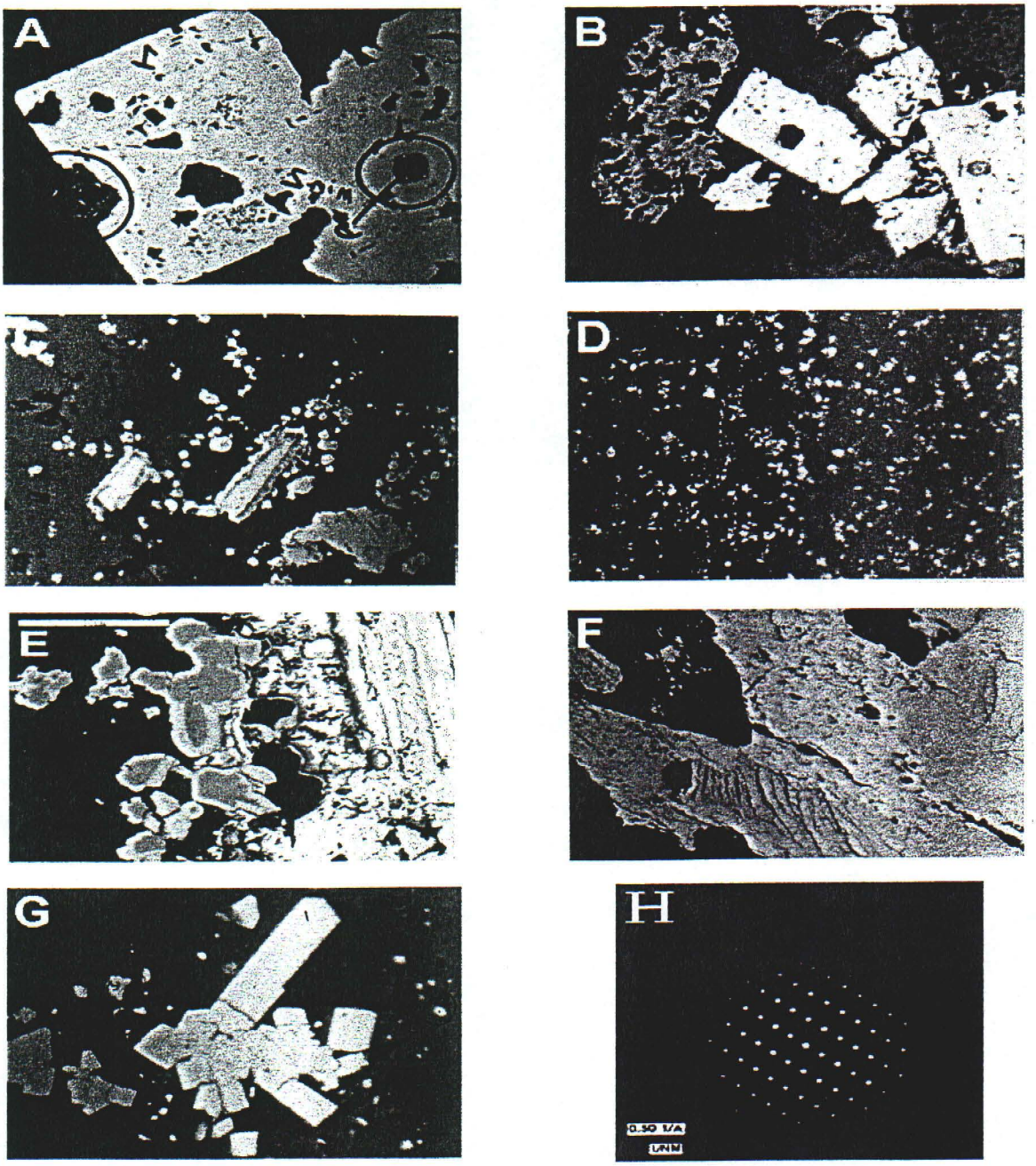

Photographs show the seven different morphologies of pyrite analyzed in this study. **(A)** coarse-grained Type 1 pyrite, rl, FOV 1600μm, **(B)** coarse-grained Type 2 pyrite, rl, FOV 1600μm, **(C)** Type 3 and 4, high-grade pyrite/marcasite rim, rl, FOV 200μm, (D) Type 3, high-grade finely-disseminated pyrite, rl, FOV 400μm, **(E)** Type 5, very high-grade pyrite/marcasite rims, BEI, FOV ~150μm, **(F)** Type 6, intermediate grade porous pyrite/marcasite, rl, FOV 1600μm, **(G)** Type 7 low-grade, marcasite, rl, FOV 200μm, **(H)** high-resolution TEM selected-area electron diffraction (SAED) image illustrating marcasite diffraction pattern,white scale bar = 0.50 1/A. Abbreviations: rl = reflected light, FOV = Field Of View, BEI = Back-scattered Electron Image.

Table 1. *EMP Trace Element Geochemistry of Pyrite*

Average Trace Element Concentrations in Pyrite (wt.%)

Pyrite Type		Fe	S	Pb	Co	Hg	Ag	Tl	Ni	As	Au	Cu	Sb	Zn	Mo
1)	1-2	46.67	55.21	0.21	0.05	0.01	0.01	0.04	0.05	0.07	0.01	0.01	0.00	0.02	0.01
2)	3	41.15	49.86	0.09	0.04	0.75	0.03	0.75	0.02	6.87	0.09	0.26	0.80	0.01	0.08
3)	4	36.03	46.82	0.00	0.03	1.05	0.00	1.00	0.19	9.30	0.08	0.32	1.46	0.00	0.00
4)	5	36.08	44.57	0.03	0.04	0.60	0.05	1.18	0.00	13.60	0.29	0.62	0.50	0.00	0.00
5)	6	44.64	52.89	0.19	0.06	0.05	0.01	0.06	0.07	1.41	0.01	0.08	0.11	0.01	0.00
6)	7	45.15	51.77	0.00	0.05	0.00	0.00	0.00	0.01	1.04	0.02	0.00	0.00	0.00	0.00

Average Trace Element Concentrations in Pyrite (wt.%)

Pyrite Type	Fe	S	Pb	Co	Hg	Ag	Tl	Ni	As	Au	Cu	Sb	Zn	Mo
7) Avg. Cores Rimmed by Type 3	45.83	54.11	0.12	0.05	0.00	0.00	0.04	0.00	0.11	0.01	0.00	0.00	0.00	0.05
8) Avg. Cores Rimmed by Type 5	43.85	52.25	0.18	0.04	0.02	0.00	0.10	0.00	2.64	0.03	0.10	0.09	0.00	0.00

Figure 9. *Trace Element Map of Type 2, 3 and 4 Pyrite*

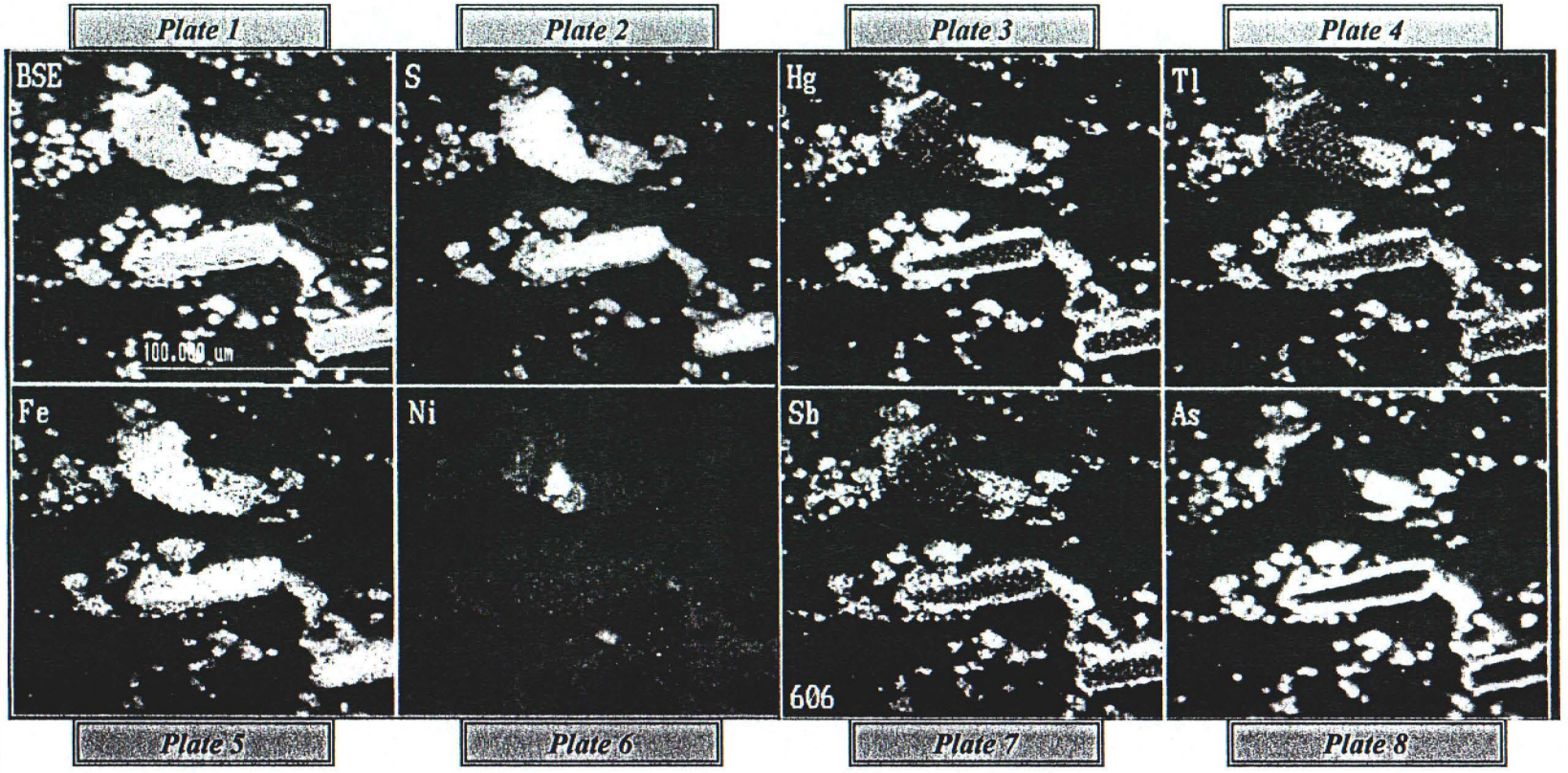

Individual trace element map dimensions are 128 X 128 pixels. EMP instrument conditions were 25 kV, 30 nA with an estimated spot size of 0.3μm. Brightness and intensity of image are equivalent to the concentration of the trace elements: white = high concentration, black = low to nil. Fe and S were mapped by Energy Dispersive Spectrometers (EDS) and Hg, Tl, Sb, and As were mapped by Wavelength Dispersive Spectrometers (WDS). Effective detection limits for EDS and WDS are approximately 1.0 and 0.1 wt%, respectively (per commun with Mike Spilde). **(Plate 1)** is a Back Scattered Electron image of a Type 2 pyrite grain, with Type 3 overgrowth, and Type 4 framboid-like sulfides in the surrounding jasperoid matrix. The structure of the Type 3 pyrite is highly visible, as it forms sharply defined rims on the Type 2 core sulfide. The Type 3 rim on the pyrite is approximately 2.5μm in width. The Type 4 framboid-like pyrite "puffballs" are visible in the ground mass surrounding the rimmed grains. **(Plate 2)** Trace element map indicates high sulfur concentrations in the brighter portions of the image, which form Type 2 cores. **(Plate 5)** Highest Fe concentrations are also indicated by brighter images in the Type 2 cores. Note the reduced brightness of Fe and S in the rims of the pyrite, indicating a decrease in the Fe and S in the trace element-enriched rims as compared to Type 2, trace element poor cores. **(Plate 6)** shows the anomalous distribution of Ni in these samples. Ni does not correlate with rims or cores. **(Plates 3, 4, 7, and 8)** are trace element maps illustrating Hg, Tl, Sb, and As concentrations, respectively, in trace element enriched Type 3 and 4 sulfides. The enrichment of these trace elements in ore-grade sulfides is evident by the brightness of Type 3 and 4 grains, and the reduced brightness of Type 2 cores. The rims of the sulfides are enriched in these elements whereas the cores are depleted in them. Note the sharp, bright Type 3 and 4 pyrite images produced by the As trace element map.

Figure 10. *Trace Element Map of Type 2 and 5 Pyrite*

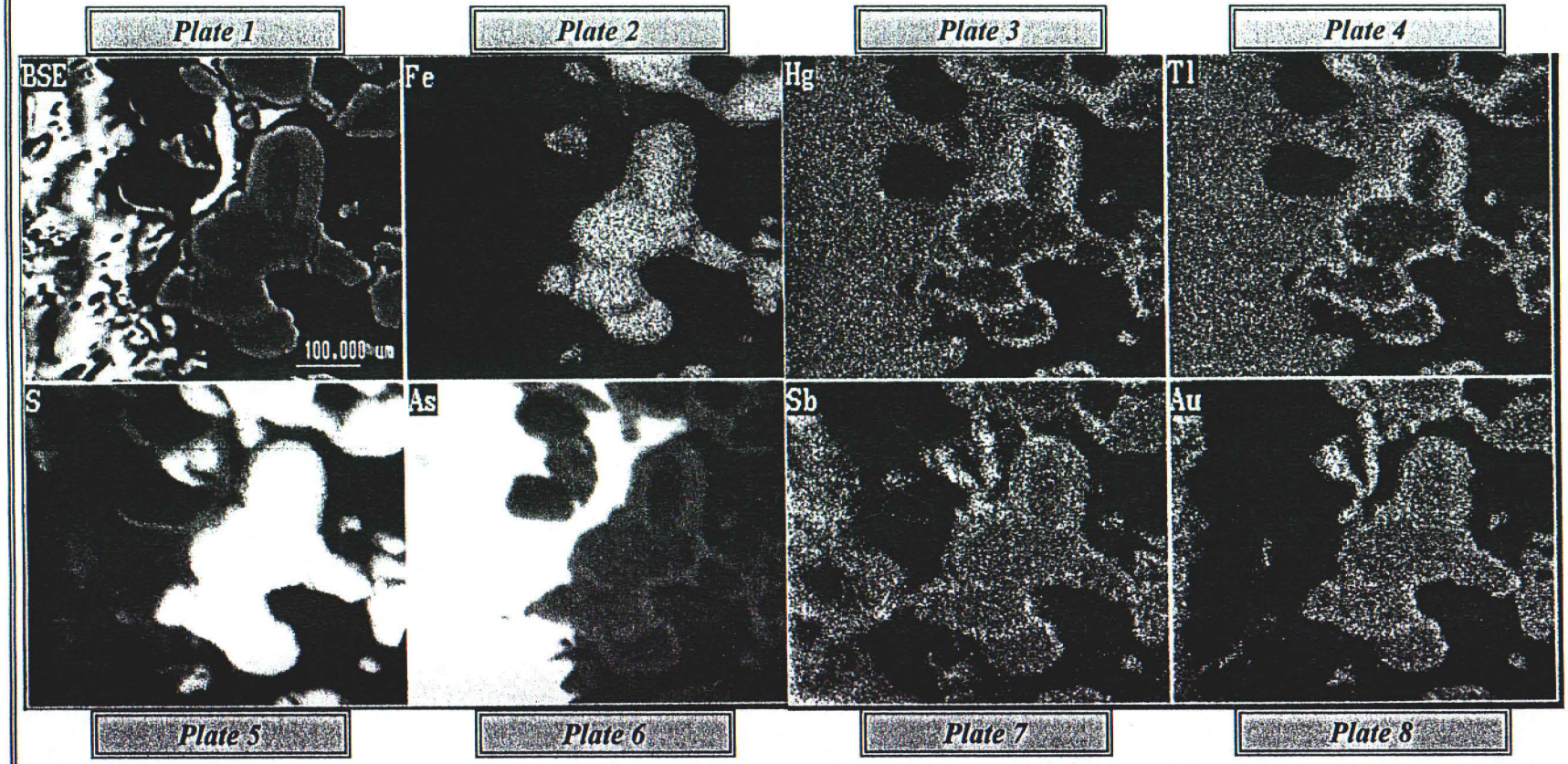

Individual trace element map dimensions are 512 X 512 pixels. EMP Instrument conditions were 20 kV, 50 nA with an estimated spot size of 0.3μm. Brightness and intensity of image are equivalent to the concentration of the trace element concentration: white = high concentration, black = low to nil. Fe and S were mapped by Energy Dispersive Spectrometers (EDS) and As, Hg, Tl, Sb, and Au were mapped by Wavelength Dispersive Spectrometers (WDS). Dwell times were 30 msec for EDS and 50 msec for WDS with 3 to 5 frames added together (per commun with Mike Spilde). Effective detection limits for EDS and WDS are approximately 1.0 and 0.1wt%. **(Plate 1)** is a Back Scattered Electron image of a Type 2 pyrite grain, with Type 5 overgrowth, surrounded by jasperoid ground-mass. The Type 5 pyrite is most evident under BEI, and does not form a sharp contact with the core Type 2 pyrite. The Type 5 rim on the pyrite is approximately 5μm in width. **(Plate 2)** Trace element map showing sulfur concentrations, indicated by brighter portions of the image in Type 2 cores. **(Plate 5)** Highest Fe concentrations are also indicated by the brighter images within the Type 2 cores. Note the less bright regions of Fe and S in the rims of the pyrite, indicating a decrease in the Fe and S in the trace element enriched rims as compared to the Type 2 trace element poor cores. **(Plate 6)** shows the distribution of As in these samples. Note: the bright region the the left of the rimmed pyrite is a realgar vein. **(Plates 3, 4, 7, and 8)** are trace element maps of Hg, Tl, Sb, and Au concentration, respectively, illustrating trace element enriched Type 5 sulfides. The enrichment of these trace elements in these ore-grade sulfides is evident by the brightness of the Type 5 rim images, and the less bright images of the Type 2 cores.

Type 6 Geochemistry: Slightly less than stoichiometric Fe and S, trace to nil Co, Pb, and Ni; trace or nil Au, Cu, As, Tl, Sb, and Hg; pyrite chemistry intermediate to low-grade Type 1-2 and high-grade Type 3 pyrite (Table 1).

Stage 3: post gold ore stage: (0.0 ounces/ton Au)

Type 7: Gold-free marcasite, bright white, rectangular to lathe shaped. Disseminated within a "dirty" opaque riddled calcite (Fig. 8G).

Type 7: Geochemistry: Slightly less than stoichiometric Fe and S, trace to nil Co, Pb and Ni; trace to nil Au, Cu, As, Tl, Sb, and Hg; Pyrite chemistry intermediate to low grade Type 1-2 and ore-grade Type 3 sulfides (Table 1).

Statistical analyses reveal strong positive correlations between Tl, Hg, As, Au, Cu, and Sb in ore stage pyrite. This suite of trace elements correlates negatively with Co and Pb. Trace elements Ag, Ni, Mo, and Zn exhibit erratic behavior, and do not correlate with the other trace elements.

Figure 11 illustrates transects from ore-stage rims through non-ore cores into ore-stage rims, and shows the negative correlation between ore-stage and non-ore stage trace elements. As varies inversely with Fe and S. Note that Pb is elevated in cores and depleted in rims, whereas Au, As, Sb, Hg, Tl and Cu are elevated in rims and depleted in cores. Co remains approximately constant across both cores and rims.

Gold Quantification

Secondary Ion Mass Spectrometer (SIMS) analyses were used to quantify submicroscopic gold and arsenic concentrations in pyrite and realgar in five samples. A total number of 41 points ~20 micrometers in diameter were analyzed on pyrite/marcasite and realgar. Analyses reveal a strong positive correlation between As and Au in ore-bearing pyrite. The data also show that fine aggregated pyrite, and fine disseminated pyrite contain the highest amounts of As and Au, occasionally at a 1:1 ratio.

Table 2. Au and As determined using SIMS.

	Type 1 & 2 sulfides	Type 3, 4, & 5 sulfides	Type 6 sulfides	Type 7 sulfides
Au (ppm)	0.44 - 0.69	78 - 2500	0.34 - 43	0.24 - 320
As (ppm)	30 - 47	20 - 2500	0.39 - 36	0.21 - 200

Depth profiles of SIMS spot analyses indicate that colloidal-sized gold microinclusions are locally present in realgar associated with pyrite (Fig. 12A). In contrast, SIMS depth profiles of fine-grained aggregated pyrite did not identify colloidal gold, suggesting that gold is, instead, in solid solution in the pyrites (Fig. 12B).

Location of Gold

High-resolution Transmission Electron Microscopy (HRTEM) diffraction patterns (Fig. 8H) reveal that fine ore-stage iron-sulfide grains are As-bearing marcasite, rather than pyrite. High resolution TEM should reveal Au in clusters and nanocrystals if Au is in the forms of inclusions; however, Au was not identified in any of the HRTEM analyses. These results are consistent with SIMS analyses, which also failed to identify the presence of gold microinclusions in pyrite.

Figure 11. *Trace Element Transect Plots*

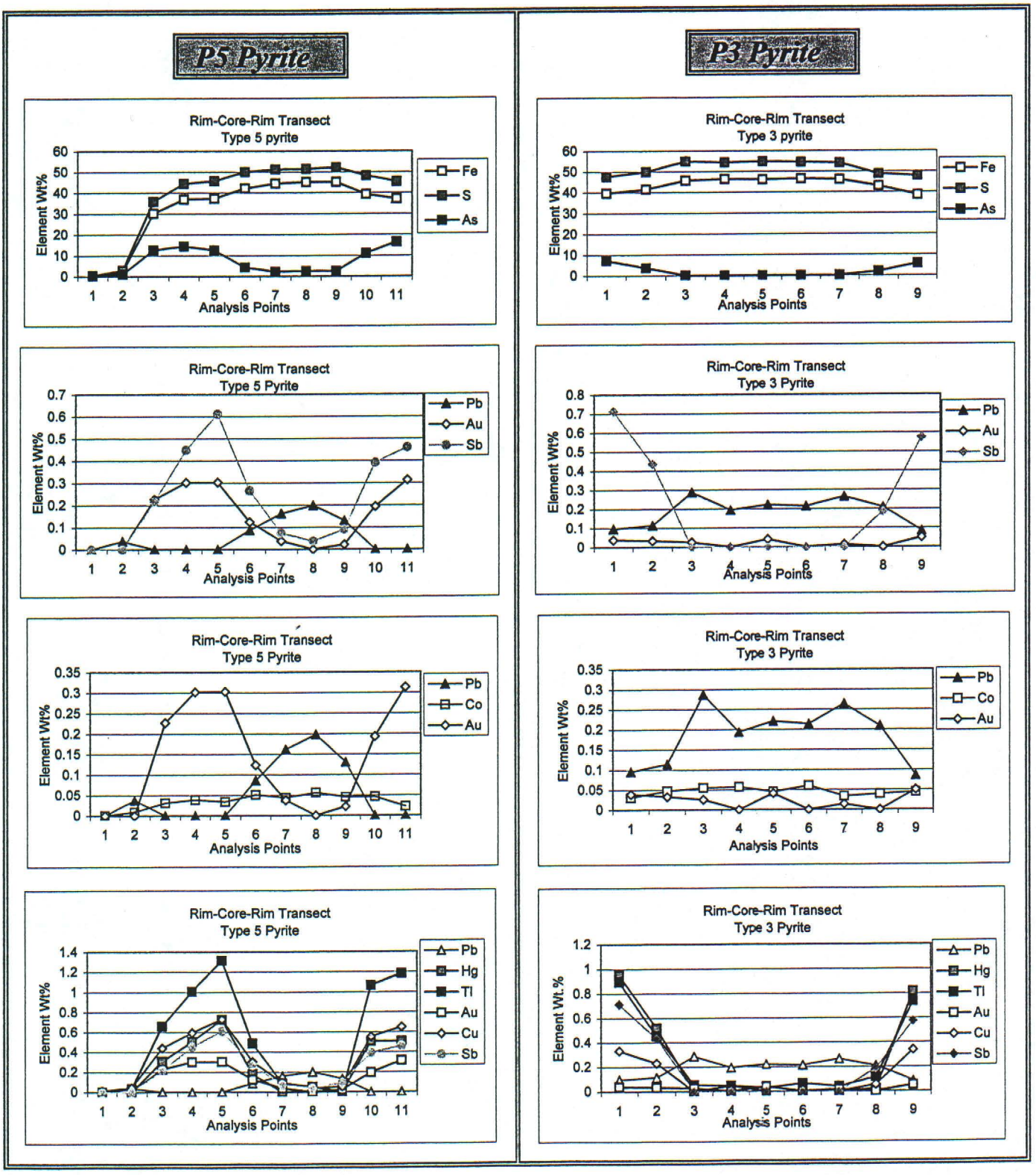

Figure 12. *SIMS Depth Profiles*

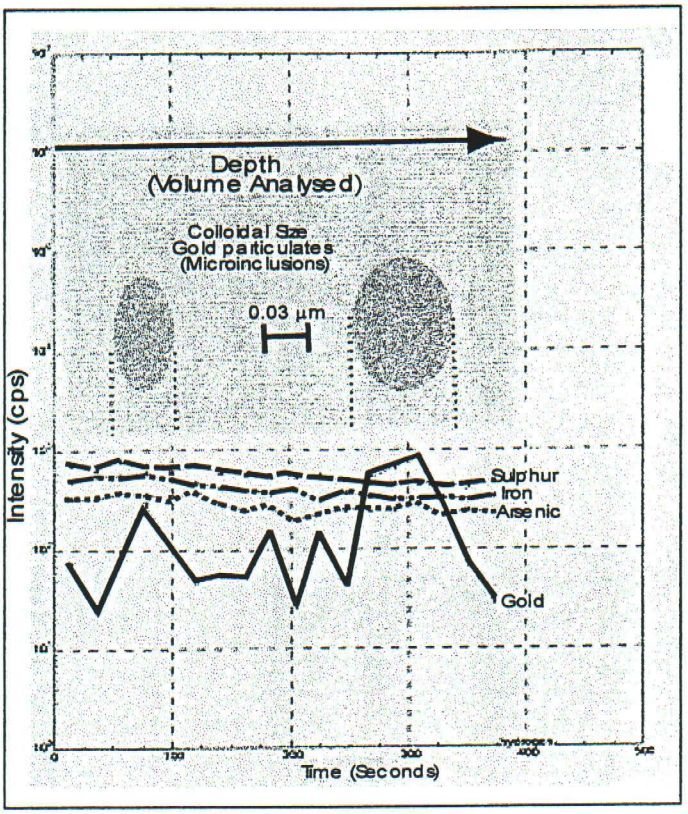

a) Depth profile of SIMS spot analysis of realgar associated with pyrite illustrating the presence of colloidal sized gold microinclusions.
The gold concentration is 556 ppm.

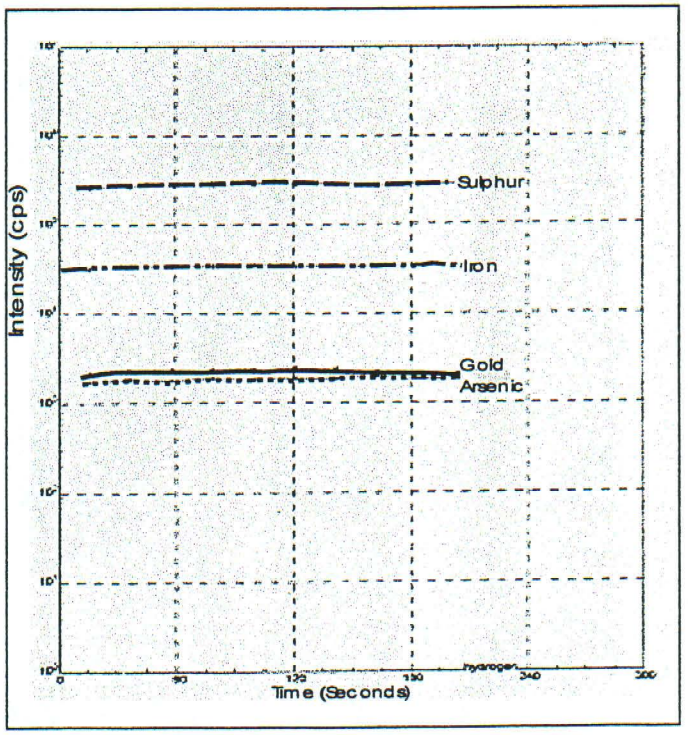

b) Depth profile of SIMS spot analysis of a fine grain aggregated pyrite illustrating solid solution gold (gold in the atomic structure of pyrite).
The gold concentration is 91 ppm,
The arsenic concentration is 87 ppm.

Preliminary Sulfur Isotope Analyses

Ten polished sections were selected for in-situ SIMS sulfur isotope analyses at Oak Ridge National Laboratory. Samples were selected to determine isotope ratios for the seven pyrite populations. Sulfur isotope analyses will indicate sources for sulfur and will contribute to identifying processes related to non-ore and ore-stage pyrite deposition.

Preliminary analyses of 5 sections have provided ranges of isotopic ratios for the pyrite populations (Table 3). Analyses have a standard range of reproducibility within 0.2 to 0.4 per mil.

Table 3. Preliminary SIMS sulfur isotope data.

Pyrite Type	δ34S Ranges	# of Analyses
1	+1.7 to +3.5	3
2	-2.1 to -0.8	4
3	-0.7 to +0.9	2
3/4	+3.3 to +7.1	5
5	+0.4 to +3.1	4
6	-7.9 to +2.2	13
7	+3.0 (small, fine lathes) to +8.9 (large, coarse cubic crystals)	3

Results to date do not lend themselves to a straightforward interpretation. Types 1 and 2 pyrites exhibit significant isotopic differences indicating that, although the two pyrite types are identical in appearance, sulfur in these pyrites does have different, possibly diagenetic and igneous, sources. Ore stage pyrite Types 3, 4, and 5 exhibit a range of values that extend to higher isotopic ratios than pre-ore stage pyrites. Low grade Type 6 pyrite has a larger range of isotopic ratios extending to very low values. Analyses of post ore-stage Type 7 pyrites indicate a difference between vein marcasite, which has lower isotopic ratios, and isotopically heavier coarse, euhedral, cubic marcasite. Isotope studies will continue in 1999.

Future Research

The geochemical data for the pyrite populations will be placed in a paragenetic framework. Results will be integrated with sulfur isotope analyses to identify formation conditions for each pyrite type. A manuscript describing the study will be prepared and submitted for publication.

ALTERATION STUDY

Project Goals

The objectives of the alteration study are: 1) to describe major, minor, and trace element concentrations in high grade ore, and 2) to determine the relationship between potassium-bearing clay minerals and the ore fluid. Oxygen and hydrogen isotope ratios of clay minerals associated with gold deposition will be evaluated to help identify the source of the fluids responsible for clay mineral deposition.

Current Research

Sampling and site analyses were completed during the summer of 1998 at the Getchell underground mine. Samples were collected from active mine locations exhibiting well-defined bedding traceable from visibly unaltered waste rock into a highly altered and mineralized zone. Sampling was restricted to a single homogeneous bed that could be followed a minimum distance of one meter from an ore zone. Individual beds are generally

between 5 and 10 cm thick and some are traceable for many meters. Approximately 80 samples were collected at measured distances from ore horizons at 12 different locations in the main and northwest ore zones. Samples include unaltered, unmineralized waste rock, moderately altered and mineralized rock, and highly altered, high-grade ore. Sampled protoliths include siltstone, limestone, and an igneous intrusive dike. Attempts were made to study the Turquoise Ridge ore deposit; however, structural discontinuities rendered it impossible to follow bedding for any significant distance at this deposit.

Samples were collected in duplicate and gold assays performed at the Getchell mine. Based on assay data, 50 samples best displaying continuation from an ore zone to unaltered waste rock were selected for further analyses. These samples were analyzed for major, minor, and trace elements at Activation Laboratories in Ontario, Canada. The concentrations of Ag, Al, As, Au, Ba, Be, Ca, Cd, Co, Cr, Cs, Cu, Fe, Hg, K, La, Mg, Mn, Mo, Na, Ni, P, Pb, Rb, S, Sb, Sc, Se, Si, Sn, Sr, Te, Ti, Tl, U, V, W, Zr, and Zn were measured for each sample. Applied analyses include inductively coupled plasma mass spectrometry (ICP-MS), inductively coupled plasma spectroscopy (ICP), instrumental neutron activation analysis, (INAA), gravimetric fire assay, and loss on ignition (LOI). In addition, total organic carbon content was measured on selected samples. Results are currently being evaluated and element mobility and immobility determined.

Polished thin sections have been prepared from 25 samples of high grade, intermediate grade, and waste rock. Examination of the thin sections has revealed the presence of characteristic Carlin-type mineralization including quartz, pyrite/marcasite, realgar, orpiment, calcite, and clay. Electron microprobe analysis has identified fine-grained carbon in sections from two separate localities. Thin sections are now being examined to determine paragenetic relationships.

Twenty samples of mineralized and unmineralized rock were taken to Sonoma State University for mineral identification using a Rigaku diffractometer with a theta theta goniometer and Jade 3.1 software. Bulk rock x-ray diffraction (XRD) was performed from 2 to 90 degrees 2 theta at a rate of 12 degrees per minute. Samples were re-run at a rate of 6 degrees per minute from 2 to 20 degrees 2 theta to attain higher resolution in the clay region. A preliminary review of the data suggests that clay minerals include montmorillonite and interlayered illite. Processes of decalcification and silicification were indicated by abundances of calcite and quartz. Analytical work and evaluation of the data will continue in 1999.

Future Research

Results of the XRD analyses will be used to select 10 pure clay samples for O and H isotope studies. Clay mineral preparation involving particle size separation and the complete removal of quartz, calcite, and organic material will begin in January. Major, minor, and trace element concentrations are being evaluated and the mobility and immobility of each element determined. Results of the chemical analyses, and XRD and isotope studies will be integrated to determine ore fluid chemistry and fluid-rock interaction in Getchell ore zones.

Acknowledgments

We are especially grateful to Getchell Gold, and particularly Dick Nanna, Mike Bauman, and Mark Gingrich, for their continued support and interest in our studies. We also thank Lee Riciputi at Oak Ridge National Laboratory for the sulfur isotope analyses, and Mike Spilde at the University of New Mexico, for assisting with the electron microprobe study.

References

Cline J. S., Hofstra, A., Landis, G., and Rye, R., 1997, Ore fluids at the Getchell, Carlin-type gold deposit, North-central Nevada, *in*, Carlin-Type Gold Deposits Field Conference, Vikre, P., Thompson, T.B., Bettles, K., Christensen, O., and Parratt, R., eds: Society of Economic Geologists Guidebook Series, Vol. 28, Littleton, Co., p. 1155-166.

Cline, J.S., Mineral paragenesis and fluid evolution at the Getchell, Carlin-type gold deposit, north-central Nevada: submitted to Economic Geology, 9/98.

DeLong, R., 1996, Geology and ore deposits of Northwestern Nevada: Geological Society of Nevada 1996 Fall Field Trip Guidebook, Special Publication No. 24, Reno, Nevada, 147 p.

Goldstein, R.H., and Reynolds, T.J., 1994, Systematics of Fluid Inclusions in Diagenetic Minerals: Society for Sedimentary Geology Short Course 31, SEPM, Tulsa, OK, 199 p.

Groff, J.A., Heizler, M.T., McIntosh, W.C., and Norman, D.I., 1997, 40Ar/39Ar dating and mineral paragenesis for Carlin-Type gold deposits along the Getchell Trend, Nevada: Evidence for Cretaceous and Tertiary gold mineralization: Economic Geology, v. 92, pg. 601-622.

Silberman, M. L., Berger, B. R., and Koski, R. A., 1974, K-Ar age relations of granodiorite emplacement and tungsten and gold mineralization near the Getchell mine, Humboldt County, Nevada: Economic Geology, v. 69, p. 646-656.

Tingley, J.V., and La Pointe, D.D., 1998, Nevada: Mining Engineering, vol. 50, no. 5, p. 92-96.